PLOS ONE

RESEARCH ARTICLE

Elasto-Capillary Folding Using Stop-Programmable Hinges Fabricated by 3D Micro-Machining

Antoine Legrain[1]*, Erwin J. W. Berenschot[1], Niels R. Tas[1], Leon Abelmann[1,2]

1 MESA+ Institute for Nanotechnology, University of Twente, Enschede, The Netherlands, **2** KIST Europe, Saarbrücken, Germany

* a.b.h.legrain@utwente.nl

Abstract

We show elasto-capillary folding of silicon nitride objects with accurate folding angles between flaps of (70.6 ± 0.1)° and demonstrate the feasibility of such accurate micro-assembly with a final folding angle of 90°. The folding angle is defined by stop-programmable hinges that are fabricated starting from silicon molds employing accurate three-dimensional corner lithography. This nano-patterning method exploits the conformal deposition and the subsequent timed isotropic etching of a thin film in a 3D shaped silicon template. The technique leaves a residue of the thin film in sharp concave corners which can be used as an inversion mask in subsequent steps. Hinges designed to stop the folding at 70.6° were fabricated batchwise by machining the V-grooves obtained by KOH etching in (110) silicon wafers; 90° stop-programmable hinges were obtained starting from silicon molds obtained by dry etching on (100) wafers. The presented technique has potential to achieve any folding angle and opens a new route towards creating structures with increased complexity, which will ultimately lead to a novel method for device fabrication.

Citation: Legrain A, Berenschot EJW, Tas NR, Abelmann L (2015) Elasto-Capillary Folding Using Stop-Programmable Hinges Fabricated by 3D Micro-Machining. PLoS ONE 10(5): e0125891. doi:10.1371/journal.pone.0125891

Academic Editor: Yogendra Kumar Mishra, Institute for Materials Science, GERMANY

Received: October 21, 2014

Accepted: March 23, 2015

Published: May 19, 2015

Data Availability Statement: All relevant data are within the paper.

Funding: The authors have no support or funding to report.

Competing Interests: The authors have declared that no competing interests exist.

Introduction

Self-folding of 3D micro-structures

The fabrication of 3D micro-structures has become an important field of interest in the scientific community over the past three decades [1]. Traditional mask-based approaches, such as photo-lithography and its developments, have proven to be inadequate for fabricating truly 3D-patterned structures. The main limitations include: an inherent two-dimensionality, size limitations, being time-consuming, and demanding a complex fabrication [2]. An alternative to mask-based techniques, methods that alter sensitive substrates have been successfully used to create 3D structures. As examples, electron beam (EB) and focused ion beam (FIB) lithographies use particles beams to achieve 3D structures with nm resolutions [3]. Femtosecond lasers allow the fabrication of arbitrary shaped 3D structures in transparent substrates. Combined

with electroplating, electrofluidic devices can be machined in glass or fused silica [4, 5]. However, these techniques remain serial and limited to compatible materials.

Fabrication examples of 3D structures abound in nature. Salt crystallization and the folding of protein or DNA are processes that engineers dream of reproducing in a laboratory with as much precision and reproducibility as is seen in nature. The process by which disordered components are organized into patterns or structures without human intervention is known as "self-assembly" or, by analogy with the previously mentioned top–down methods, a "bottom–up" approach [6]. Although great proofs-of-concept have been published [7, 8], such engineering suffers from a too high level of uncertainty, as pointed out by Gracias *et al.* in their excellent review [1]. Therefore, they prefer the use of a more deterministic form of self-assembly known as "self-folding" or "micro-origami". Combining the strengths of both lithography and self-assembly, the final 3D structure is predetermined by the linkages between the different parts that are assembled. The obvious link with origami, the ancient Japanese art of folding paper, provided its name to this technique [9]. While origami-like planar structures are fabricated using standard micro-machining techniques, many methods of self-folding have been investigated, some more efficient than others. These methods include ultrasonic pulse impact [10], pneumatics [11], electroactive swelling [12, 13], thermal actuation of polymer films [14–17], thin-film stress-based assembly (TFSA) [18–22], magnetic forces [23–27], and capillary forces. Surface tension is probably the most common method of self-folding. In the micro/nanometer world, interfacial forces dominate over body forces such as gravity, making them a perfect candidate for the self-folding of micro-structures. Syms was the first to introduce this method by using solder pads which are melted to power assembly before solidification in their final state [28, 29]. More recently, this method has had great nanoscale applications as a result of the work of Gracias *et al.* [30–32]. For a complete overview of self-folding techniques, see the recent reviews [1, 33–35].

An elegant macro-scale illustration of self-folding by surface-tension is Bico *et al.* [36–38], who demonstrated the spontaneous wrapping of thin millimeter-sized polydimethylsiloxane (PDMS) sheets around a water droplet: the so-called elastocapillary folding technique. Using the same concept, our group has demonstrated the fabrication of silicon nitride 3D micro-objects by capillary forces in which the actuating liquid, in our case water, disappears as a result of its spontaneous evaporation. Final closure is assured by the strong cohesion between flaps without the need for solder, and the assembly is carried out under ambient conditions either by simply depositing water on top of the structures [39] or by providing a liquid through a tube at the centre of the objects [40].

A crucial feature of self-folded objects is to pre-determine their final shape. Some techniques require a locking mechanism, for example, some research on self-folding by magnetic interaction [23, 25], while another treatment of magnetic self-folding relies on plastic deformation [27]. Using solder assembly, the quantity of melting material determines the final folding angle [28, 30, 41]. Likewise, in TFSA, the final radius of curvature is a function of the stresses in the different layers, with curvatures ranging from a few millimeters down to nanometers [18–20]. The final shape from using self-folding polymer films can be controlled by designing several small shrinking hinges in series [15, 16, 35].

Structures folded by elasto-capillary interactions are limited in terms of their final three-dimensional shapes. Folding ceases once the moving flaps encounter an obstacle, typically a nearby flap. The structures will reopen after the liquid has evaporated if the bending energy stored in the hinge exceeds the adhesion energy between the flaps [36, 39, 40]. This adhesion energy is commonly in the order of 1 mJ m^{-2} [55]. The elastic energy per unit surface stored in the hinges depends on their bending stiffness and folding angle. In the experiments presented in

this paper, this energy is two orders of magnitude smaller than the adhesion energy, so the structures will remain closed.

The work presented here aims at extending the scope of elastocapillary folding of silicon nitride micro-objects by predefining the final assembly. The principle of these stop-programmable hinges is presented in Fig 1.

Made of a thick rigid part and a thin flexible part, these complex hinges are designed in such a way that the final assembly angle is predefined by their shape. After folding through evaporation of water, the two opposite thick parts meet and adhere. The final folding angle therefore depends on the initial angle between the substrate and the thick parts of these smart hinges.

Corner lithography and self-folding

Corner lithography is a wafer scale nano-patterning technique that offers the opportunity to form structures in sharp concave corners, independently of their orientation in space. The conformal deposition of a material layer over a patterned substrate will result in a greater effective thickness in any sharp concave corner. Isotropic etching therefore yields nano-features as presented in Fig 2.

This technique was first developed and used in our laboratory to create silicon nitride nanowire pyramids [42]. We then extended the scope of this technique by demonstrating the use of the structures formed by corner lithography as a mask for subsequent patterning steps [43]. In the meantime, Yu *et al.* demonstrated the fabrication of nano-ring particles and photonic crystals using corner lithography [44]. More recently, our group has continued the development of this technique and demonstrated the parallel nano-fabrication of fluidic components with cell culturing application [45], as well as the wafer-scale fabrication of nanoapertures [46] and the machining of silicon nitride 3D fractal structures [47].

In this paper, we use corner lithography to fabricate the smart hinges presented in Fig 1. Sharp features must be avoided when it comes to bending or folding, since they lead to an extreme concentration of stress [48, 49]. Consequently, corner lithography needs to be performed in rounded molds for our purposes. This situation leads to conditions on the radius of curvature of the mold, as well as on the thicknesses of the subsequently deposited material. In general, the total thickness of the materials that are deposited in rounded molds must be greater than their radius of curvature so as to have some material remaining after the isotropic etching, as shown in Fig 3.

Materials and Methods

In this section we present the fabrication steps necessary to build the stop-programmable hinges depicted in Fig 1. The main steps are the same for the fabrication of both folding angles, although 90° stop-programmable hinges require the use of wet etching to pattern the vertical sidewalls, unlike the 70.6° complex hinges, for which everything can be accessed by dry etching. Moreover, methods to obtain the molds differ. The two following sections extensively describe the process flow, with the first part describing the whole procedure for 70.6° smart hinges, and the second part pointing out the differences when fabricating 90° stop-programmable hinges.

We use silicon rich nitride (SiRN) as the body material for the hinges because it is hydrophilic, its deposition techniques and properties are well-known in the semiconductor industry, as well as its demonstrated robustness [39, 40]. SiRN is preferred over stoichiometric nitride (Si_3N_4) because of a lower tensile stress, making it more suitable as a construction material. SiRN deposited by low-pressure chemical vapor deposition (LPCVD) has been fully characterized in our cleanroom in the past [50] and the deposition equipment is subject to regular tests to ensure continuity in its properties. Our last tests in date on the material yielded a Young's

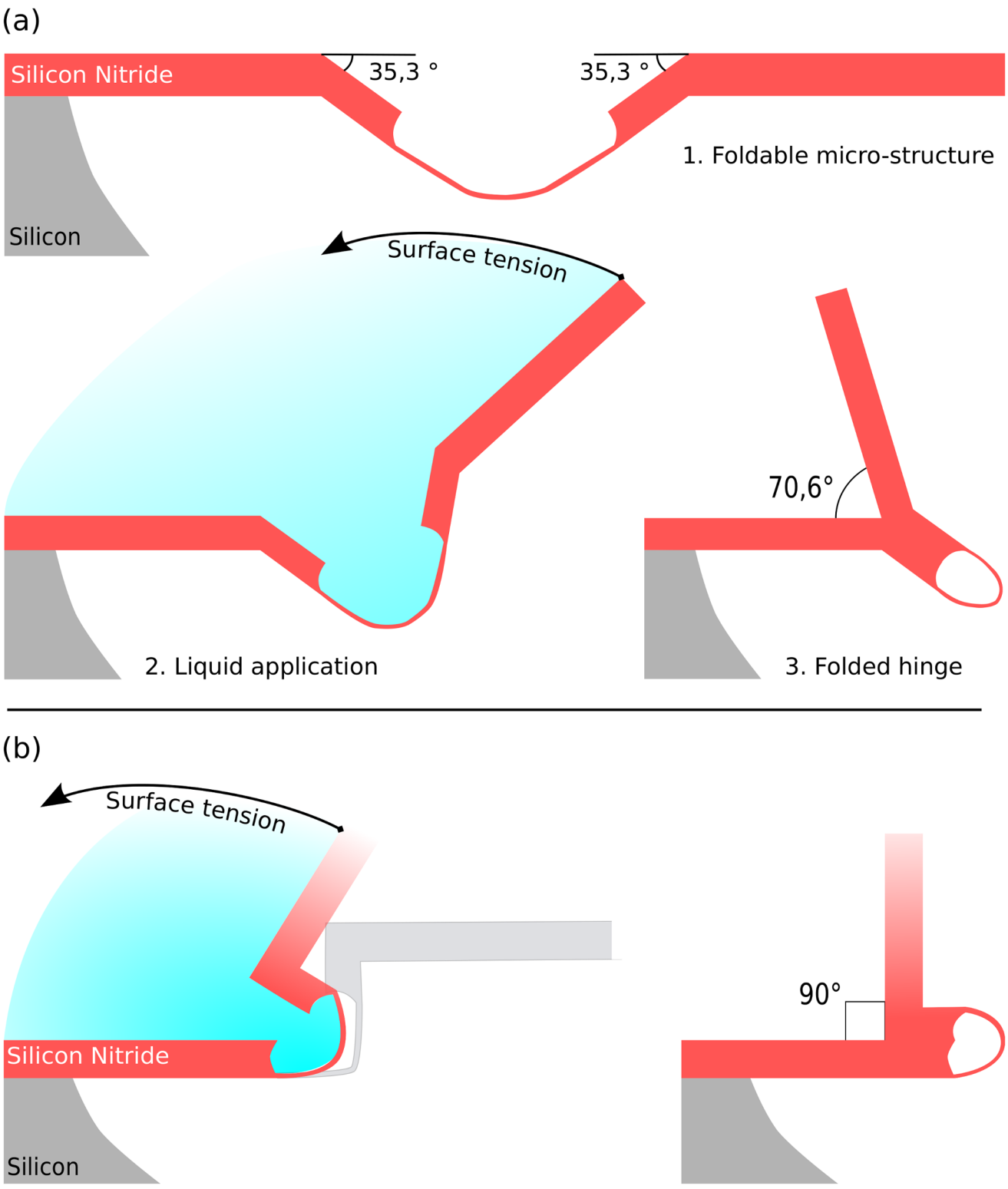

Fig 1. Stop-programmable folding principle. The design of the complex hinges is such that once folded, the flap forms a predefined angle with the planar support. Self-folding of the structure is enabled through evaporation of water and decrease of the liquid–air interface of the meniscus. (a) 70.6° stop-programmable hinge. (b): 90° stop-programmable hinge. In both cases, the flaps adhere due to a sufficiently large stiction area and there is no need for a locking mechanism.

doi:10.1371/journal.pone.0125891.g001

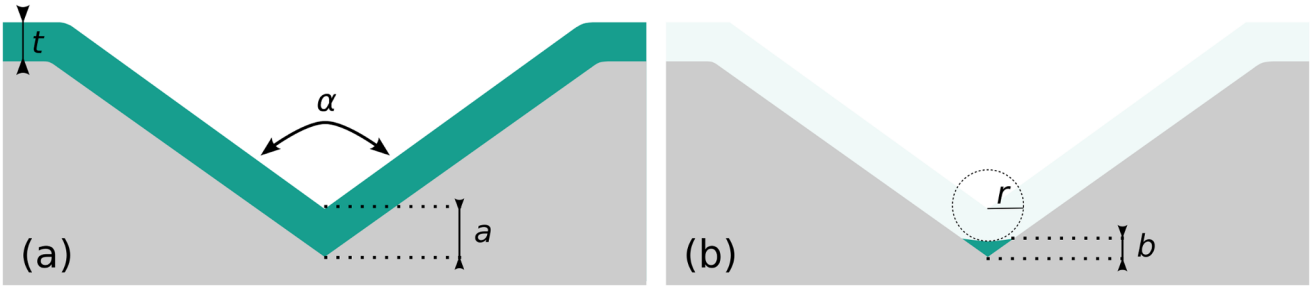

Fig 2. Corner lithography in a sharp corner. (a): When a conformal layer of thickness t is deposited over a concave corner of opening α, the effective thickness of material at the corner is $a = {}^{t}/_{\sin(\alpha/2)} > t$ [42]. (b): After isotropic etching by an amount of r, material with thickness $b = a - r$ remains in the corner.

doi:10.1371/journal.pone.0125891.g002

modulus of (290 ± 45) GPa (resonance frequency measurement) and a tensile stress of (−169 ± 25) MPa (wafer curvature method). These results are in accord with values found in the literature. In addition, the quality of the deposited layer is checked after every deposition run using a cold light source to find possible imperfections and by ellipsometry (observed refractive index $2.14 < n < 2.16$).

70.6° stop-programmable hinges

The strategy is similar to that presented by our lab in previous publications [43, 45]. Corner lithography is here employed to create a masking layer which will be subsequently used to etch the underlying body layer before being removed. Fig 4 shows the procedure step by step for machining a 70.6° stop-programmable hinge.

The initial Si (silicon) molds will define the shape of our final object. The opening angle α of the molds, see Figs 2 and 3, defines the final folding angle, β, through the relation $\beta = \pi - \alpha$. Silicon has a face-centred cubic structure with a well-defined lattice. The angle between the top $< 110 >$ plane and the {111} planes is exactly 35.3°, as depicted in Fig 1. Etching the molds with KOH on (110) oriented wafers yields well-defined openings with the desired opening angle ($\alpha = 109.4°$, $\beta = 70.6°$) with sharp transitions between the different planes, see Fig 4(a). Note that the mask pattern, consisting of rectangular openings, needs to be rotated by 54.7° with respect to the vertical $< 111 >$ planes in order to get rectangular V-grooves with KOH etchant.

The bending of sharp objects is to be avoided since it leads to extreme stress concentrations [48, 49]. We therefore use an oxidation step to round off the molds, Fig 4(b). Kim *et al.* showed

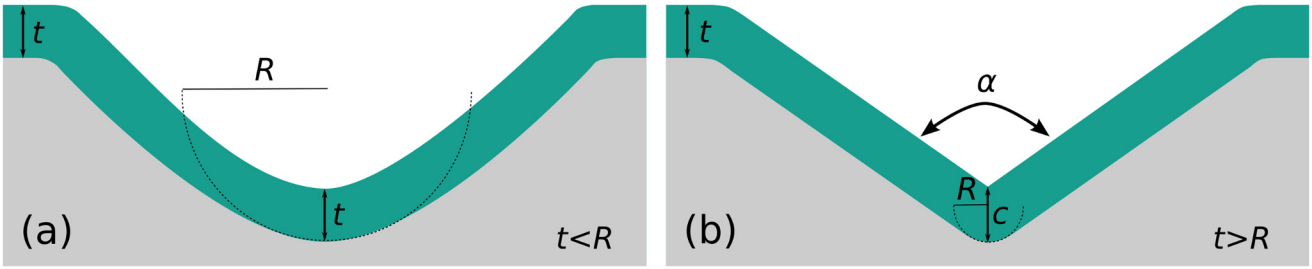

Fig 3. Corner lithography in a rounded corner. (a): When a material layer of thickness t is conformally deposited over a mold with radius of curvature R that is greater than t, the thickness at the tip is unchanged. (b): On the other hand, when R is less than t, a concave corner is created and the effective thickness is $c = R + {}^{(t-R)}/_{\sin(\alpha/2)}$.

doi:10.1371/journal.pone.0125891.g003

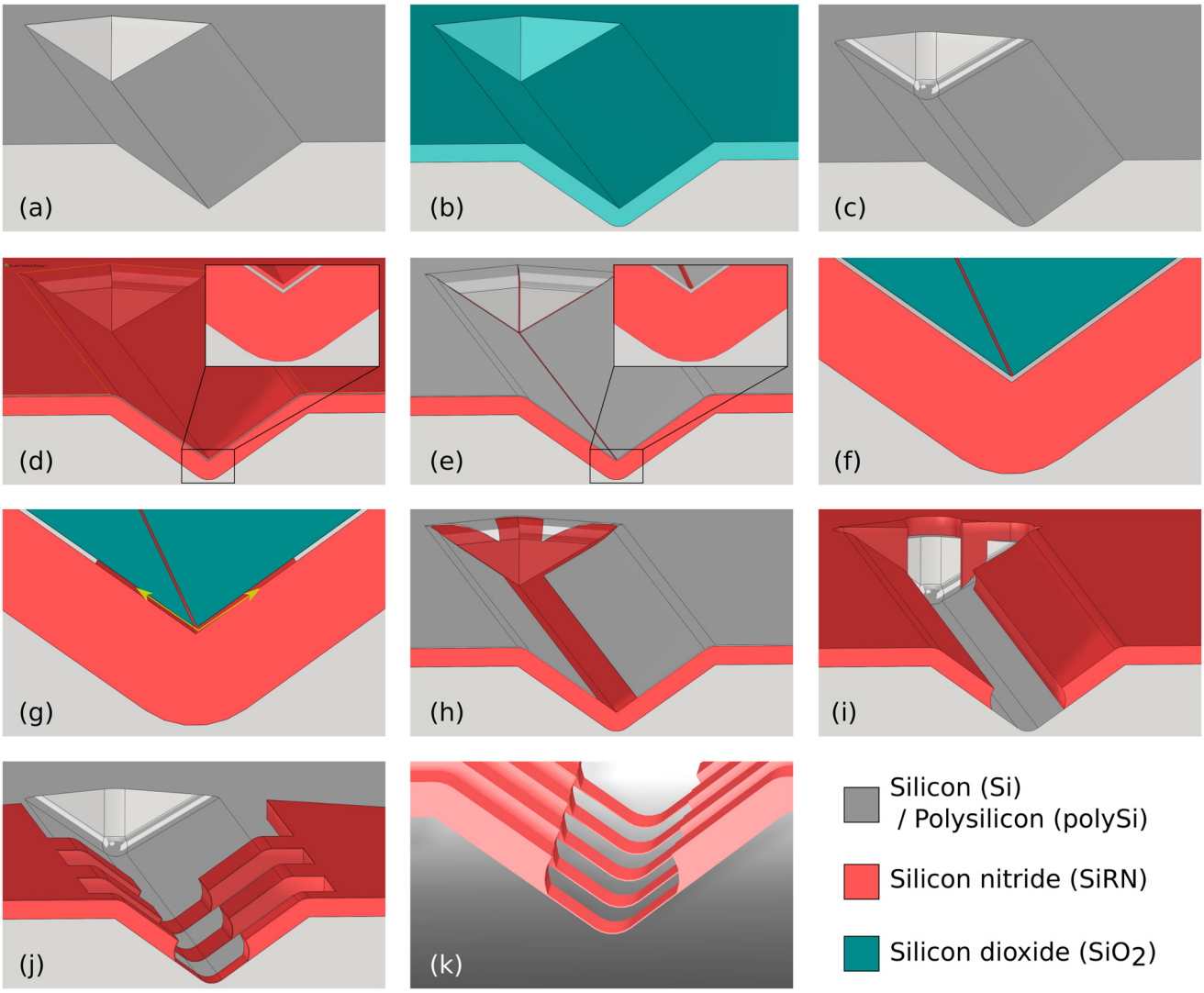

Fig 4. Fabrication of a stop-programmable hinge, example of a 70.6° smart hinge. (a): On a (110) oriented silicon wafer, V-grooves are etched. (b) and (c): These grooves are rounded off by means of oxidation and subsequent etching. (d): A SiRN/polySi/SiRN stack of layers is conformally deposited. (e): The top SiRN layer is isotropically wet etched using a time stop such that material remains in the corner. SiRN wires run in all three directions. (f): This remaining SiRN nanowire is used as a protection mask during partial oxidation of the underlying polySi layer. (g): After removal of the SiRN line the polySi layer is retracted. (h): SiO_2 is stripped. (i): Using the polySi layer as a mask, an opening is etched in the SiRN layer. An oxidation and subsequent wet etching step follow to remove the polySi layer (not shown here). (j): After deposition of flexible layer of SiRN, a mask is applied through lithography and the overall geometry of the structure is determined by directive ion etching. (k): A last lithography step follows for protection of the SiRN objects during semi-isotropic etching of Si. Once released from the substrate, the smart hinge is ready to be self-folded.

doi:10.1371/journal.pone.0125891.g004

that high temperature oxidation is an efficient method to round off sharp silicon V-grooves [51]. Linear relations between the oxidation time and the final achieved radius of curvature were experimentally found by the authors for (100) oriented wafers but not for (110) wafers. Our own oxidation experiments followed by SEM inspections allowed us to determine a similar relation for a 1150°C wet oxidation step applied to (110) wafers:

$$R = (124 \pm 72) + (94 \pm 7)\sqrt{t} \quad (1)$$

with R the final radius of curvature in nm and t the oxidation time in min. A 98 min oxidation step yields a 1 μm radius of curvature and is used for our fabrication, Fig 4(b). It is difficult to use a higher radius of curvature since that would imply a deposition of a thicker material layer, as described in Fig 3(a). Once SiO_2 (silicon dioxide) is stripped in HF, the molds are ready for corner lithography.

First, two layers are deposited by LPCVD: first, a thick SiRN layer that is to be structured to form the thick part of the smart hinges, see Fig 1, followed by a polysilicon (polySi) layer. The total thickness of material here needs to be greater than the initial radius of curvature R as was emphasized in Fig 3. Typically, we deposit a 1 μm SiRN layer and a 150 nm polySi layer in a mold where the radius of curvature R is 1 μm. In any case, the following design criterion should be respected:

$$t_{\mathrm{SiRN}-1} + t_{\mathrm{polySi}} \geq R \tag{2}$$

where $t_{\mathrm{SiRN\text{-}1}}$ and t_{polySi} stand for the thickness of the bottom SiRN and the polySi layers, respectively.

On top of this stack, a last conformal layer of SiRN is deposited. Provided that the design criterion has been respected, the cross section of the stack should look like Fig 4(d). There are no constraints on the thickness of the top SiRN layer, but it needs to be perfectly known since this layer will be time-etched in phosphoric acid ($H_3\,PO_4$) to form SiRN nanowires at the bottom of the grooves as shown in Fig 4(e). In the case of a $\alpha = 109.4°$ opening, the material is 22% thicker at the tip (see Fig 2) and over-etching of the SiRN layer is allowed within this limit. We have used a thin SiRN layer of about 100nm to reduce the etching time.

Thanks to the newly formed nanowires running in the three dimensions, the underlying polySi layer can be partially oxidized (Fig 4(f)) using SiRN nanowires as an inversion mask. Half of the polySi thickness can be consumed during this step without issues. Once the nanowires are selectively etched, the polySi layer can be retracted starting from the tips where nicely defined access points are now formed, step (g). TMAH as an etchant is a nice option here since its selectivity between SiRN and SiO_2 is high and the etching speed not too fast to be controllable, but KOH could also be used. Careful timing is necessary during the retraction, since the length of the flexible parts of the smart hinges are determined during this step, see Fig 1. Typically, a TMAH solution at 25wt% at 95°C attacks polySi at a speed of 1 μm min^{-1}.

The above steps result in a patterned polySi layer on top of the thick SiRN layer, Fig 4(h). Using the polySi layer as a mask, it is now possible to etch the underlying SiRN layer in HF 50%. Due to the isotropic nature of the etchant, a retraction equal to the thickness of the material etched will occur under the polySi masking layer. Moreover, when the thickness of the SiRN layer to be etched is greater than the initial radius of curvature R, an over-etching is necessary to remove the surplus material (Fig 3), its thickness can be calculated by

$$c = \frac{(t - R)}{\sin\left(\frac{\alpha}{2}\right)} \tag{3}$$

with t the thickness of the conformal layer and α the opening angle of the mold.

In order to remove the polySi masking layer, an oxidation step should be preferred over a wet etching step since we want to conserve the rounding of the mold. This short oxidation step will consume the polySi material and slightly increase the radius of curvature of the mold. Moreover, the oxidation of the Si substrate will yield a specific shape, known as a bird's beak, at the transition between the Si and the SiRN [52]. This shape is not visible in Fig 4 but will be shown in the results part of the paper (Fig 10).

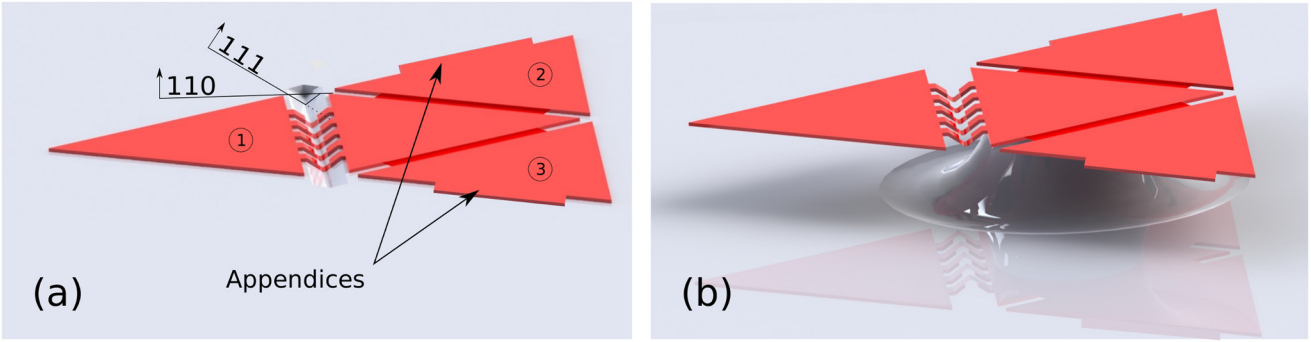

Fig 5. Fabrication of a tetrahedron folding pattern, extra steps. (a): Since only one of the hinges lies on the correct intersection of the planes, standard lithography is used to define flat hinges for the other faces. Faces 2 and 3 are designed with small appendices on their sides to allow them to lock onto face 1 while folding. (b): Under-etching of Si by semi-isotropic etching of silicon (SF_6 etchant). Etching is stopped when the hinges are free and the central flap rests on a silicon pillar.

doi:10.1371/journal.pone.0125891.g005

After removal of the polySi layer, Fig 4(i), the flexible part of the hinges is deposited by LPCVD. The bending stiffness of the hinges is $B = {Et^3}/{12(1-\nu^2)}$ for thin plates, where E is Young's modulus and ν is Poisson's ratio [53]. It is highly dependent on the thickness t of the thin plate, and the thinner is this layer, the more flexible is the hinge. 100 nm thin hinges offer both mechanical solidity and flexibility [39, 40]. On the other hand, the final release of the foldable objects requires the etching of the Si molds in SF_6, which also slightly attacks SiRN. The thinning of the hinges during the release step should therefore be taken into account when depositing the thin SiRN layer. We measured a selectivity of around 1000 between silicon and SiRN using our etching system (Adixen AMS100 Reactive Ion Etcher).

A second lithography step follows to define the overall geometry of the smart hinges. Making holes along the length of the hinges permits reducing their stiffness and facilitates the folding. Lithography in molds up to 10 μm deep is relatively straightforward when using an appropriate photoresist. In this specific case, dry etching can be used to remove the SiRN, step (j). An extra lithography step must be performed to protect the SiRN structures by photoresist during the semi-isotropic etching of the silicon. Once released from the silicon substrate, the stop-programmable hinges are ready for assembly. When designing the masks, extra care was taken to assure that all structures were etched free from the substrate at the same time during the last step. Ideally, the mask openings should be of the same size and placed at the same distance from the stop-etching point.

The 70.6° stop-programmable hinges thus fabricated can be used to self-fold perfectly defined tetrahedrons. Since only one out of three hinges in a tetrahedron pattern lie at the right intersection between the planes in the silicon lattice, as shown in Fig 5, only one smart hinge can be formed in the way that was just described. The other two hinges are therefore flat junctures made by standard micro-machining. An extra lithography step followed by dry etching is therefore necessary between steps (i) and (j) in Fig 4.

90° stop-programmable hinges

The procedure to fabricate 90° stop-programmable hinges is nearly the same as for the 70.6° hinges described above, except for two important differences: making 90° molds in silicon is very difficult using wet etching—our attempts using correctly oriented (110) wafers always resulted in tiny bumps at the bottom edges of the molds—and the vertical SiRN sidewalls

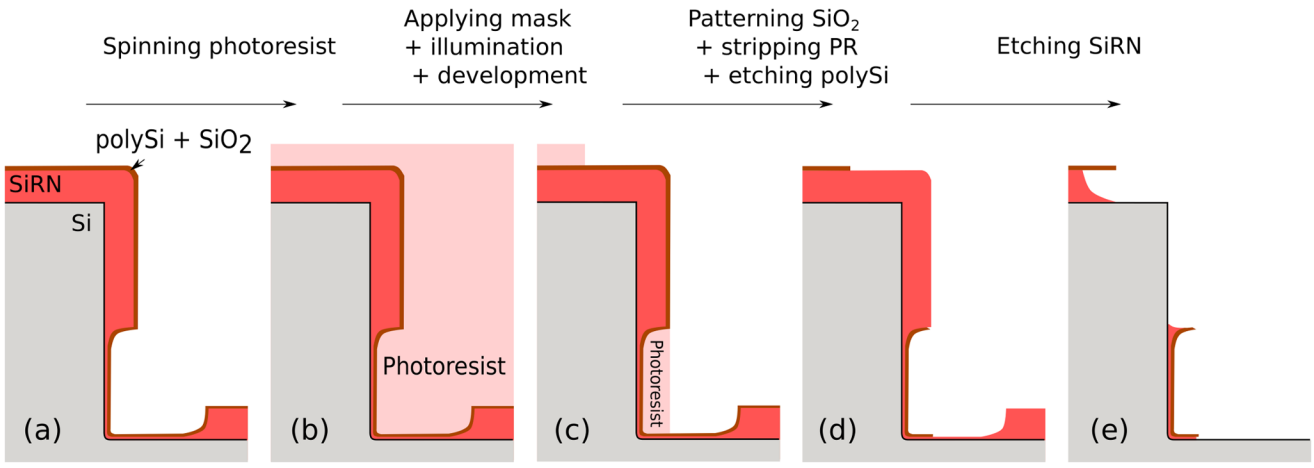

Fig 6. Difficulties arising when implementing corner lithography in an upright mold. We consider the case where the process flow depicted in Fig 4 has been followed up to step (i) inclusive. (a): Dry etching is impossible, a wet etching strategy must be considered using a masking layer. A polySi layer is deposited followed by short oxidation. (b): Photoresist is spun over the wafer. The use of a thick photoresist dedicated to high-aspect ratio structures protection is necessary to protect the molds. (c): Directional nature of UV illumination makes impossible the proper patterning of photoresist under the thick SiRN plate. (d): Consequently, the masking layer is not etched away everywhere. (e): SiRN is still present all around the molds at their bottoms.

doi:10.1371/journal.pone.0125891.g006

obtained in these molds cannot be patterned using directive dry etching. Steps (a) and (i–j) in Fig 4 therefore differ when it comes to the micromachining of 90° stop-programmable hinges.

Given that the depth of the molds is small, cryogenic dry etching is a good option for our purpose. Unlike the BOSCH processes, cryogenic etching yields smooth sidewalls [54], which are crucial for our sensitive corner-lithography technique. Retraction of the mask is also a well known problem in dry etching and might be an issue for corner-lithography. In general, when developing a dry etching step for the purpose of performing corner lithography later on inside the molds, any concave corners other than the ones at the bottom of the molds should be avoided. This includes potential roughness of the masking material and retraction of the mask. Moreover, the final opening angle α is highly dependent on the etching conditions (type of mask used, loading, gas flows) and requires precise tuning.

After performing the corner lithography, it is necessary to pattern the SiRN features before releasing the structures, Fig 4(i)–4(j). While reactive ion etching is a perfect option for 70.6° stop-programmable hinges, it is impossible to use it in the case of the vertical molds obtained by dry etching. The difficulties arising with upright sidewalls are twofold, as shown in Fig 6. One is the difficulty to etch several μm of material from the top. And the other is the vertical thick SiRN plate of the complex hinge, see Fig 1, that makes impossible a proper illumination of the photoresist for the subsequent lithography steps. Therefore an alternative method must be considered.

We suggest here to pattern the vertical sidewalls in two main steps, which are shown in Fig 7. Since it is impossible to illuminate the photoresist when it is masked by the thick upright part of the hinge, both parts of the hinges cannot be simultaneously patterned. The whole thick SiRN plate must be patterned first by wet etching before depositing the flexible part. In order to avoid an extra masking layer deposition and time-consuming wet etching step, the already patterned polySi layer by means of corner lithography, Fig 4(h), can be used for this purpose. A short oxidation step is performed to form a $\simeq 5$ nm SiO_2 layer on top of the polySi. A lithography follows to define the overall geometry of the foldable objects. SiO_2 is then patterned in

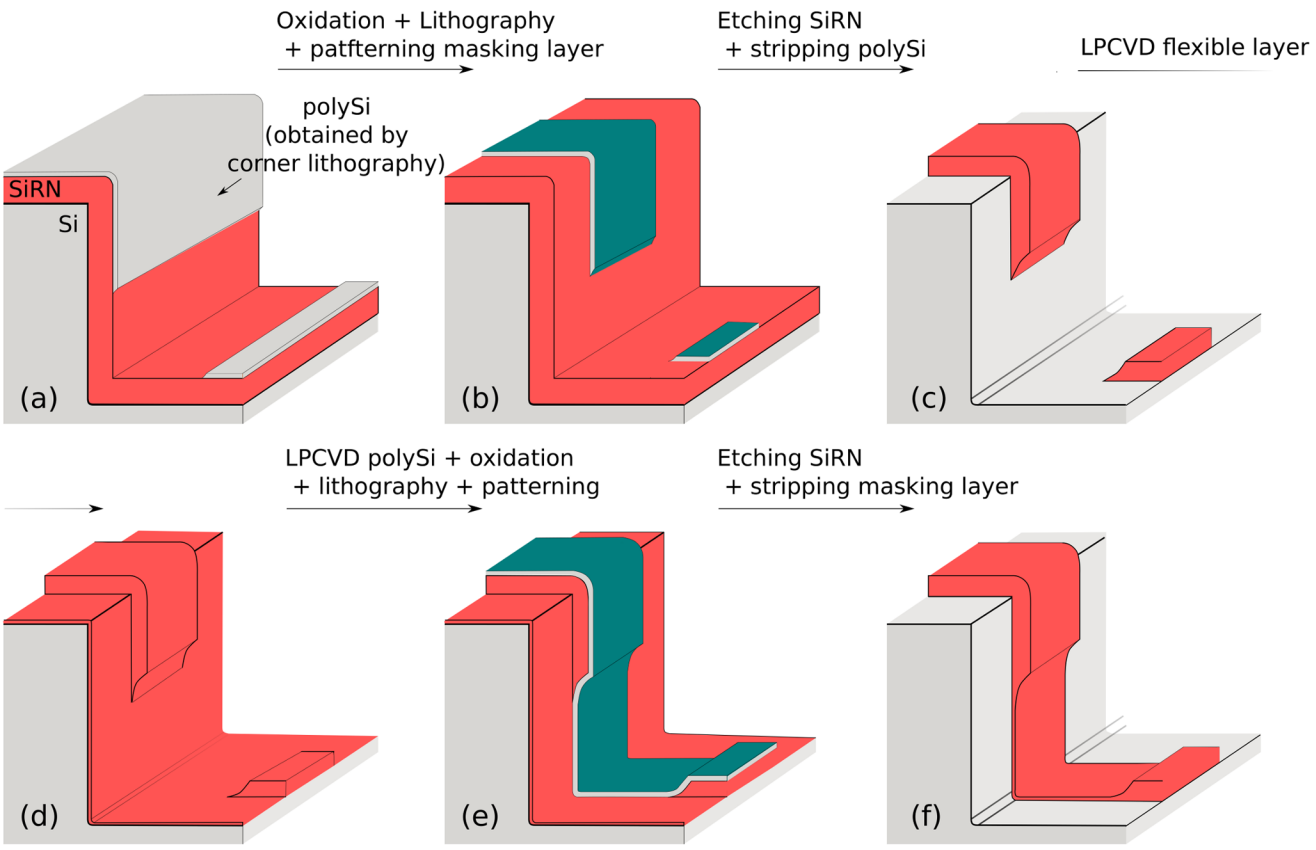

Fig 7. Alternative steps to pattern upright sidewalls. (a): The thick SiRN should be patterned first. The polySi masking layer obtained thanks to corner lithography can be used. (b): A short oxidation step follows to form a thin SiO_2 layer. Unlike in Fig 6, lithography is possible to pattern the masking layer. (c): SiRN is wet etched using the oxidized polySi as a masking layer. PolySi is fully oxidized and stripped. (d): A flexible SiRN layer is deposited by LPCVD. (e): After LPCVD of a polySi layer followed by a short oxidation, the mask used in step (b) is applied a second time to pattern the masking layer. (f): SiRN is wet etched and the masking layer stripped. The origami patterns are now complete with no SiRN wire running anywhere around the mold as was the case in Fig 6.

doi:10.1371/journal.pone.0125891.g007

three dimensions in wet etchant BHF. After stripping the photoresist, TMAH is used to pattern the underlying polySi using the SiO_2 layer as a mask, Fig 7(b). The thick SiRN layer is then accessible and can be selectively etched, independently of the spatial direction.

After the conformal deposition of a thin SiRN layer (150 nm, Fig 7(d)) followed by a polySi layer (100 nm), the exact same procedure can be applied again: short oxidation of polySi, second lithography using the same mask, patterning of oxide and polySi etching, Fig 7(e). Wet etching of thin SiRN and final stripping of masking polySi layer follow to complete the origami patterns, Fig 7(f).

The use of wet etching induces that the SiRN layers are etched under the polySi masking layers. The structures will therefore be attacked twice from their sides, in steps (c) and (f) in Fig 7.

Results

Fabrication results—70.6° stop-programmable hinges

Fig 8 illustrates the design criterion introduced in Fig 3 and described in Eq 2. By varying the oxidation time, two molds with different radii of curvature were made (Fig 4(b)) and subjected

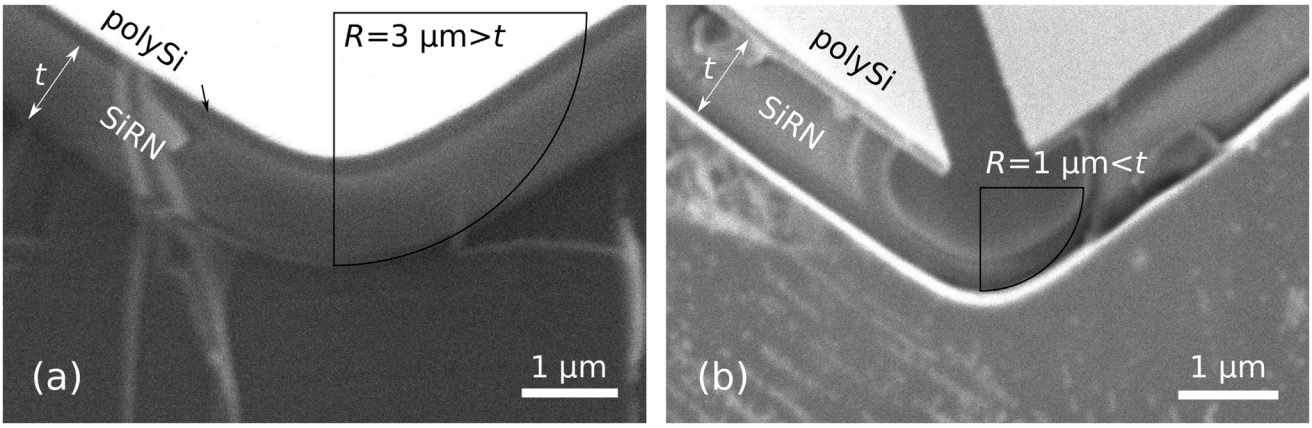

Fig 8. Illustration of the design criterion described in Fig 3. Figs. (a) and (b) show samples with different radiis of curvature for the initial mold after performing corner lithography and partially etching the bottom SiRN layer, Fig 4(i). The thickness t of the first deposited SiRN layer is 1.1 µm. (a): When $R > t$, the entire surface of the polySi layer was oxidized during step (f), consequently the retraction, step (g), had no effect. (b): For $R < t$, the polySi layer is opened and the underlying SiRN layer can be etched, Fig 4(i).

doi:10.1371/journal.pone.0125891.g008

to the exact same fabrication steps until the isotropic etching of the bottom SiRN layer (Fig 4 (i)). Since the thickness of the stack of the layers in the first case does not exceed R, there is no concave corner at the bottom of the groove. Consequently, the timed-etching step of the top SiRN layer (Fig 3(f)) does not yield nanowires and the entire polySi layer is oxidized during the subsequent step (g). Without access points below the nanowires, no retraction can occur. Once the oxide is stripped, a non-patterned thick SiRN and polySi layer stack is obtained, as can be seen in Fig 8(a).

In the correct case of Fig. (b), the radius of curvature R is smaller than the thickness t of the SiRN layer. The entire etching procedure can proceed and yields a clear opening in the polySi layer through which SiRN can be etched.

Corner lithography is a powerful three-dimensional patterning technique. The trick works for concave corners of any size and spatial configuration. As an illustration, Fig 9 shows the

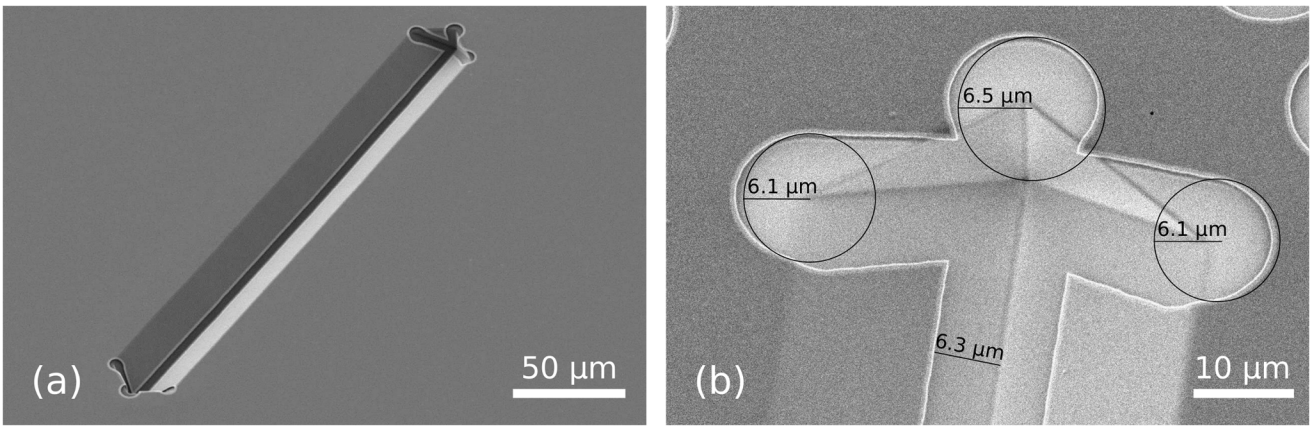

Fig 9. Retraction step. (a): Overview of a V-groove after etching of the SiRN layer, Fig 4(h). (b): Zoom in the extremity of the groove after stripping away the polySi top layer, Fig 4(i). Retraction occurs in all concave corners, including the vertical planes. The retraction length is the same in every direction.

doi:10.1371/journal.pone.0125891.g009

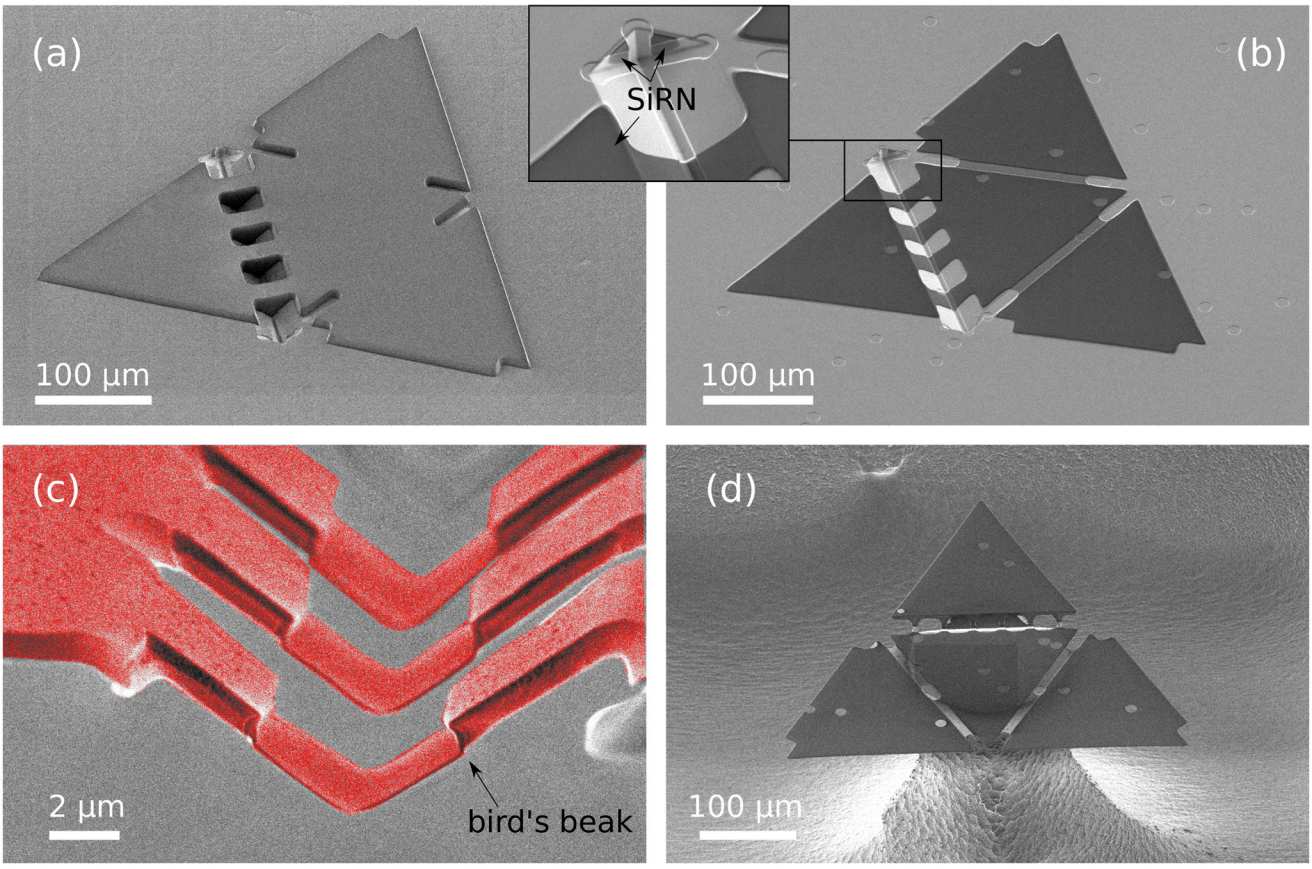

Fig 10. SEM images of final fabrications steps. (a): Tetrahedral pattern of thick photoresist. (b): SiRN template after over-etching in the grooves and stripping of photoresist. The combination of a complex hinge with two flat hinges can be observed, see Fig 5(a). (c): Close-up image of a complex hinge after the silicon mold was etched away in dry etching and the photoresist stripped, Fig 4(k). (d): Overview of an unfolded tetrahedral structure at the end of the process. Isotropic etching of Si is stopped once the pattern comes to rest on a central pillar, Fig 5(b). Note that this structure is not completely released, since Si is still present under the flaps.

doi:10.1371/journal.pone.0125891.g010

result when starting from V-grooves made by anisotropic etching in KOH. The planes are organized in a well known fashion, and the use of corner lithography leads to retraction in all three dimensions.

Fig 10 gives an overview of the last fabrication steps of a tetrahedral pattern. The use of a thick photoresist developed for high aspect ratio features is necessary for good protection of the deep V-grooves during the dry etching of the SiRN features, Fig 4(j). The result obtained with AZ 9260 photoresist is good, as shown in photographs (a) and (b). Such planar protection is obtained by coating and spinning the resist at 300rpm for 10s then 60s at 2400rpm. The resist is exposed three times for 10s at intervals of 10s and is developed for 7min. As can be seen in the inset of picture (b), SiRN remains on the upright sidewalls after the dry etching step: only the top part was attacked by reactive ion etching. These small SiRN spots are, however, not a problem for our folding structures.

As is visible in pictures Fig 10(a), 10(b) and 10(d), pinholes were present all over the wafer. They originate from nanoscopic defects in the bottom SiRN layer that turn into microscopic features because of the corner lithography: another proof of the extreme sensitivity of the technique. As long as the pinholes appear on the flaps and leave the hinges intact, they do not

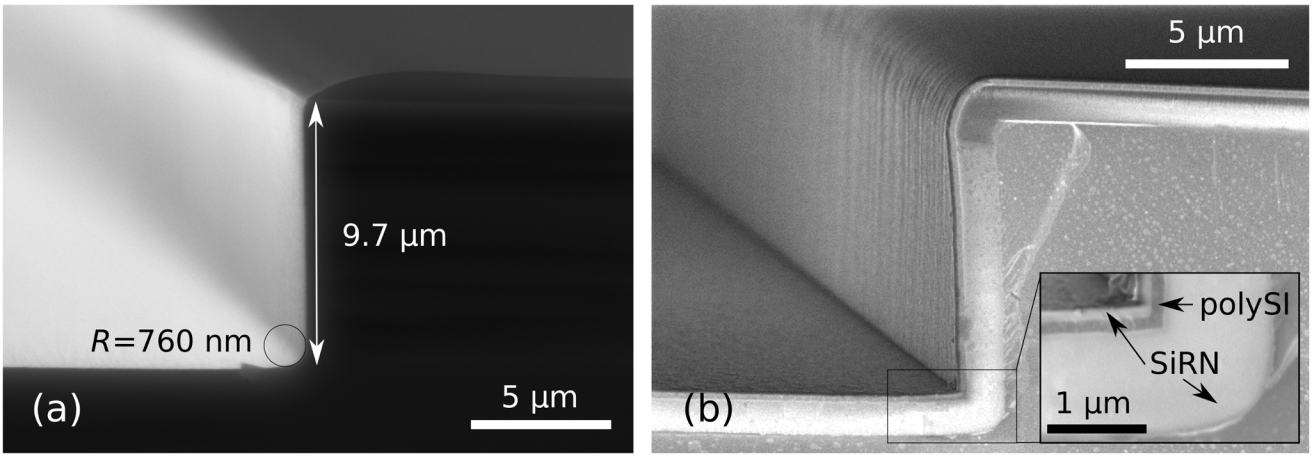

Fig 11. First steps of 90° complex hinges fabrication. (a): Cross section of a mold obtained by dry etching of silicon. The corner is not exactly perpendicular (measured to be 89°) and the process yields a round corner. These parameters can be modified by fine tuning the dry etching step. Note that photoresist is still present on top. (b): Stack of the three layers necessary for corner lithography: thick SiRN (1070 nm), polySi (around 150 nm) and a second layer of SiRN (146 nm).

doi:10.1371/journal.pone.0125891.g011

represent an issue for our folding purposes. However, the quality of the first SiRN layer should be checked at the beginning of the fabrication.

The stop-programmable hinge shown in Fig 10(c) is nearly identical to the schematic presented in the process flow, Fig 4(k), except for the small bumps visible at the transitions between the thin and the thick parts of the smart hinges. These transitions are called 'bird's beaks' because of their characteristic shapes [52], and originate from the oxidation step necessary to remove the polySi layer between steps (h) and (i) in Fig 4.

A nearly released tetrahedral pattern is presented in Fig 10(d). A circular protection of photoresist was present on top of it before the release step in SF_6, Fig 4(k), hence the circular shape of the Si pillar.

Fabrication results—90° stop-programmable hinges

As was emphasized in Part 1, the fabrication for both stop-programmable hinges is identical except for the creation of the molds and for the final etching of the SiRN layers.

Our best results for getting molds using dry etching are presented in Fig 11. We used a mixture of SF_6 (200sscm) and O_2 (15sscm) gases at -110°Celsius (Adixen AMS100 Reactive Ion Etcher, pressure 1.6d-2mbar, RF 200W, LF 20W on/off time 25/75ms). The dry etching step yields a rounded mold, picture (a), which reduces the oxidation time necessary to get the final desired radius of curvature. The depth of the molds was checked on six different spots spread over one dummy wafer and was found to be the same as that depicted in Fig 11 within an error of 5%. Photograph (b) shows a similar mold on top of which the three layers necessary for corner lithography were deposited, Fig 4(d). Since the design criterion (Eq 2) is respected, the rounding has disappeared after the conformal deposition of the first SiRN layer.

In Fig 11(b), the defects of the initial mask can be observed on the vertical sidewalls. In order to avoid undesirable corner lithography starting points at that location, the over-etching of the top SiRN layer (Fig 4(e)) was deliberately long. The corners formed due to irregularities of the mask have large opening angles, so the surplus of material is thinner than in the 90°

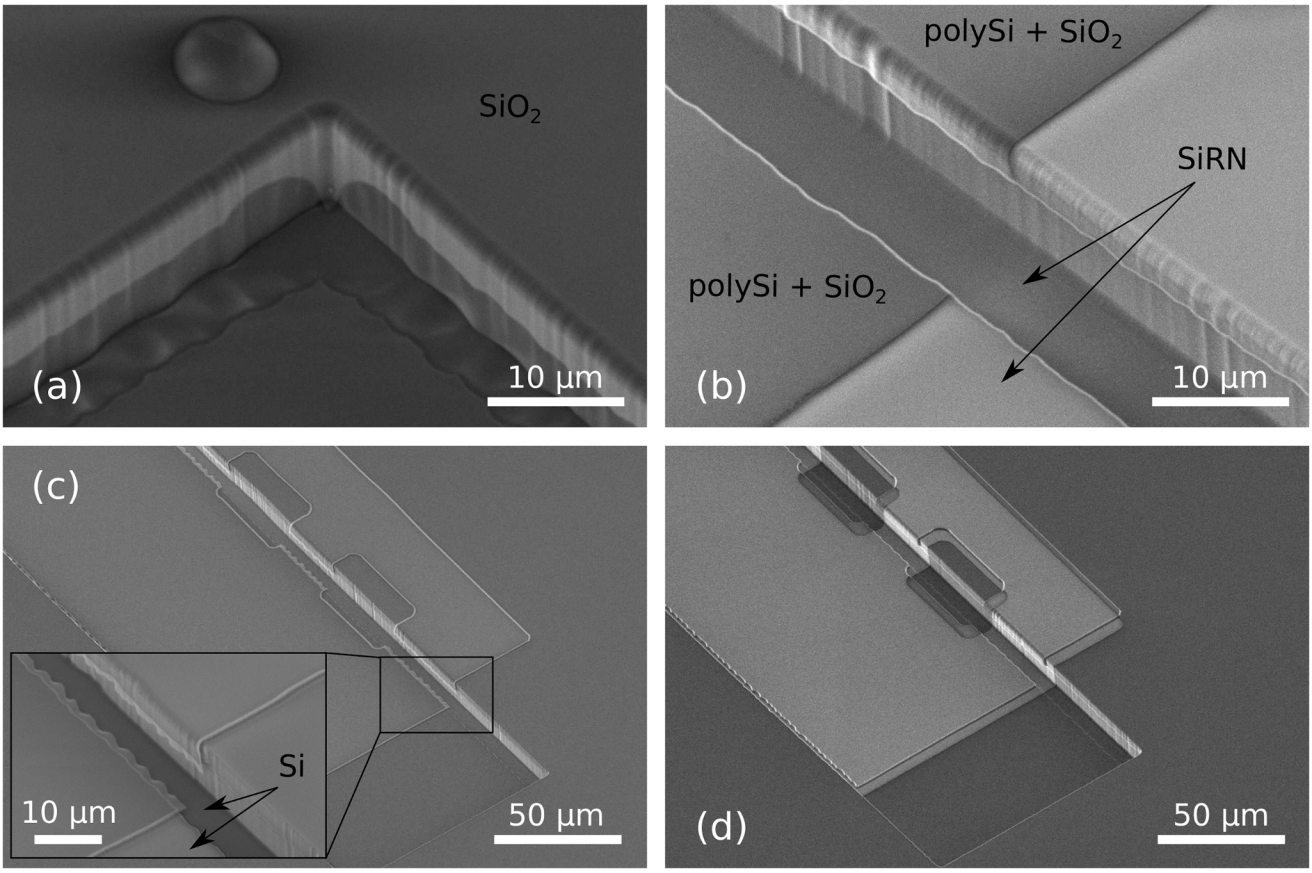

Fig 12. SEM images of fabrication steps for 90° complex hinges. (a): Retraction of polySi is visible under SiO_2, Fig 4(g). The polySi plate is not exactly straight. These irregularities are exact replicas of the defects of the silicon mold, which have been magnified through corner lithography. (b): Thick SiRN with patterned masking partially oxidized polySi layer on top. (c): Same as (b) right after wet etching of SiRN. Stress in SiO_2 mask causes the curtain-like overhanging thin film. (d): Final structure before release after the second wet etching procedure was applied.

doi:10.1371/journal.pone.0125891.g012

corners at the bottom of the grooves. Since in a perpendicular corner the material is in theory 41% thicker (see Fig 2), a 25% over-etch was performed.

Fig 12 shows the subsequent steps in fabricating 90° stop-programmable hinges. The successful retraction after the corner lithography is shown in photograph (a). Unlike the results presented in Fig 9, no retraction occurred on the top or in the corners of the mold. This is a consequence of the long over-etching explained in the previous paragraph. This long over-etch of the top SiRN layer when performing corner lithography removed all unwanted material in the irregularities of the molds, as well as in their corners.

As explained in Part 1, dry etching cannot be used in the case of upright molds and a double wet etching strategy must be used. Fig 12(b) shows the patterned masking layer, corresponding to step (b) in Fig 7. The oxidized polySi layer following the retraction shown in (a) was further shaped by oxidation and subsequent lithography steps. This way, the material at the bottom of the molds is etched and the geometry of folding patterns is defined simultaneously. Picture (c) shows the resulting structures after SiRN etching, with only the flexible part of the hinges missing, see Fig 7(c). The same wet etching procedure is applied a second time after depositing a thin SiRN and polySi layer, resulting in the structures shown in photograph (d), Fig 7(f).

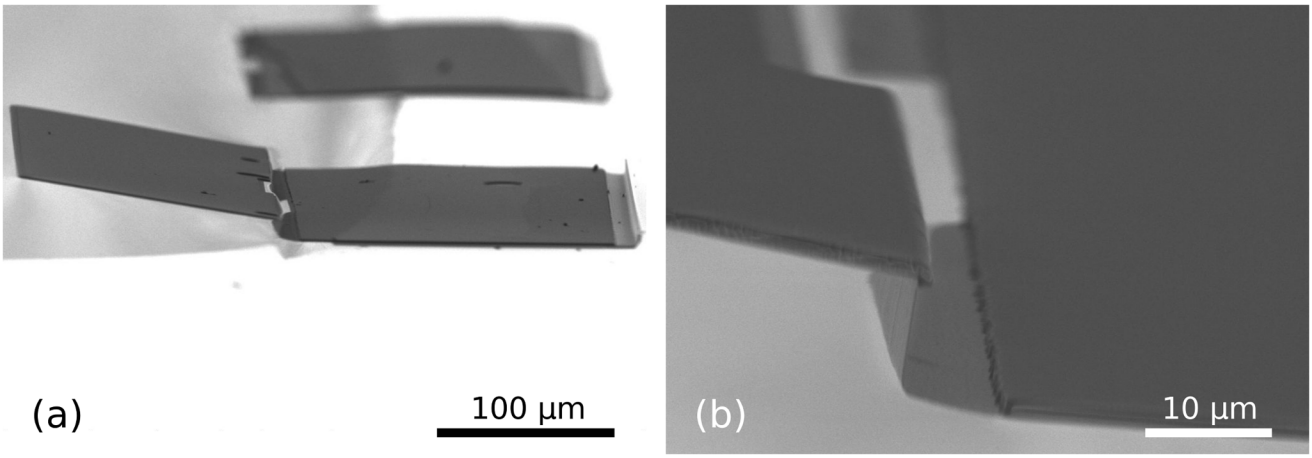

Fig 13. Final structure before folding. (a): Residual stress in the thin SiRN layers provoked a slight bending upward of the flap. (b): Zoom in at a stop-programmable hinge.

doi:10.1371/journal.pone.0125891.g013

Misalignment of the mask in the second lithography step on top of the first patterned SiRN explains the staircase-like shape of the final SiRN object.

Fig 13 shows a self-foldable object released from the Si substrate, similar to the structure in Fig 12(d). The fabrication was in principle successful, except for the fact that the length of the landing part of the complex hinge is extremely small in comparison with the flexible part, see Fig 1.

Folding experiments

Self-folding experiments were carried out by manually depositing water droplets of 5 to 15nL. An accurate positioning system allowed us to deposit the liquid right at the centre of the templates using a hollow fibre (50 µm diameter) connected to a high precision Hamilton glass syringe filled with ultra pure water that was manually actuated. The folding of the structures typically takes around one minute, depending on the size of the structures and the volume of liquid deposited.

Fig 14 shows the results of successful folding experiments. Fig. (a) shows a wing folded at the designed angle of 70.6°. Fig. (b) shows a tetrahedron resting on a silicon pillar. The large contact areas between the thick SiRN parts provide a good stability for the 3D objects after drying. The tetrahedral structure was folded from a similar pattern presented in Fig 5(b) and Fig 10(d). One stop-programmable hinge makes sure that the folding stops at 70.6° while large appendices designed on the side of the other faces allow them to lock onto the first flap.

Fig 15 shows the folding results when using 90° smart hinges presented in Fig 13. These results are less successful. A too long retraction of the polySi during the corner lithography, coupled with the wet etching steps necessary to pattern the final objects, led to wrongly shaped complex hinges. The thick parts of the hinges are too small, and the folding did not stop at all (a), or stopped too late (b). However, these results are encouraging and demonstrate that 90° stop-programmable hinges are feasible. Reducing the TMAH retraction to 2 µm, which would lead to 4 µm long flexible plates, would most probably be sufficient for a successful assembly.

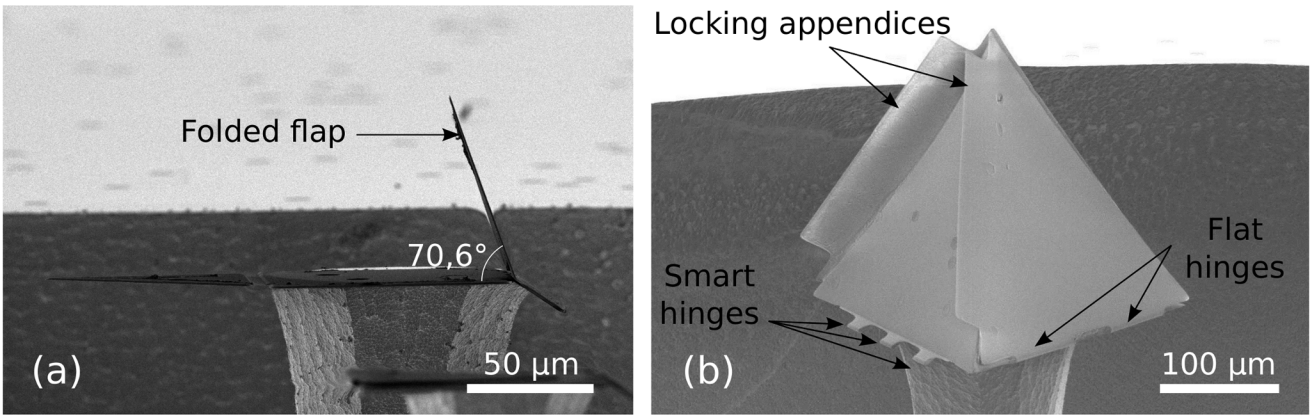

Fig 14. Folded structure arrested by 70.6° stop-programmable hinges. (a): Side view of an extruded-2D structure. The flap is 100 µm wide and the complex hinge has an original width of 40 µm. The flap of the left hand side, connected with a flat hinge, reopened after folding because of an insufficient bonding area. (b): Folded tetrahedron. The faces have sides of 200 µm, the complex hinges are 20 µm wide and the flat hinges are 10 µm wide.

doi:10.1371/journal.pone.0125891.g014

Discussion

The technique presented in this paper was first successfully used to fabricate 70.6° stop-programmable hinges. The same principle was then applied to upright molds, but issues were encountered during the process. Difficulties with the molds (retraction of the mask and roughness) caused our first attempt to fail. However, it became straightforward to perform corner lithography in 90° molds when a long over-etching was used. We initially used a 1.05 times over-etching in the case of 70.6° stop-programmable hinges and increased it to 1.25 for 90° complex hinges. Later on during fabrication, difficulties in patterning upright sidewalls forced us to modify the process. Dry etching of SiRN with rotated samples, as well as a single wet

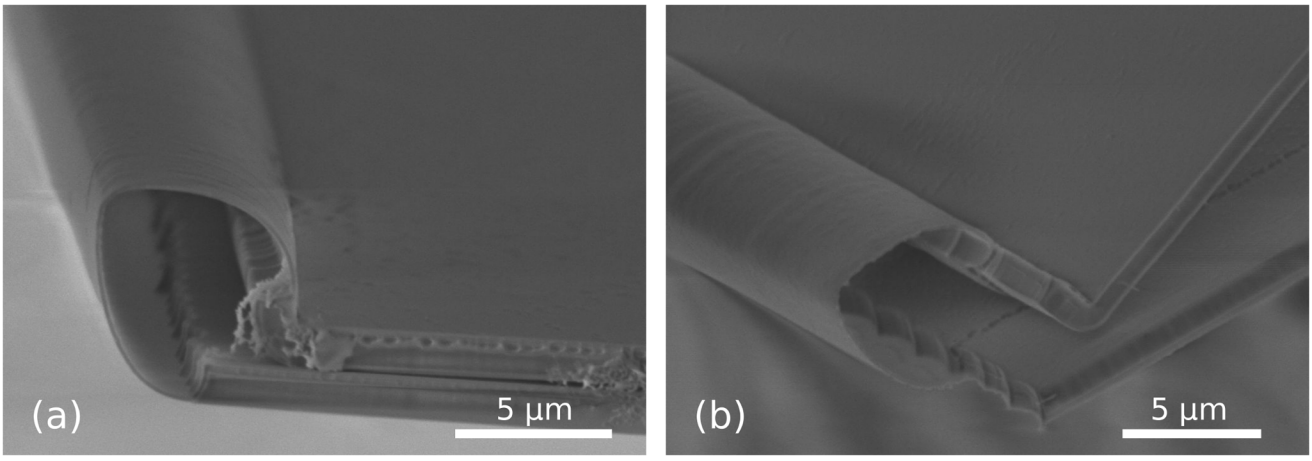

Fig 15. Folding results of 90° stop-programmable hinges. (a): The thick part of the complex hinge is too short ((1.8 ± 02) µm) and fails to stop the folding. Consequently, the flap is 180° folded. (b): For this sample, the thick part is slightly longer ((3.2 ± 02) µm). This forces folding to stop at an intermediate position, but fails to stop the folding at 90° as was intended.

doi:10.1371/journal.pone.0125891.g015

etching step, were first unsuccessfully carried out before coming up with the appropriate two-step wet etching patterning strategy described here.

The results presented here are encouraging. As long as the necessary molds can be obtained in Si, the procedure that has been described in this paper is applicable to virtually any folding angle. In principle, the wet etching method for patterning SiRN onto the sidewalls should be applied for any mold opening angle $\alpha \leq 90°$, while dry etching should be preferred when $\alpha > 90°$.

Elastocapillary folding allows the assembly of relatively large structures. The characteristic capillary length, $\lambda_c = \sqrt{\gamma / \rho g}$ (here, γ is the surface tension, ρ is the density of the fluid, and g denotes the gravitational acceleration), gives an indication of the scale on which capillarity is dominant over gravity. For clean water and air at standard conditions, the transition is around 2mm. Elastocapillary folding of several mm long silicon-based objects is therefore theoretically possible. It is known to be hard to fabricate features of this size out of the wafer plane by conventional two-dimensional micro-fabrication techniques. Indeed, 2mm is more than four times the standard thickness of a standard silicon wafer. 90° stop-programmable hinges are especially interesting since they would permit popping up several mm long features out of the plane of the silicon wafers exactly where the hinges are designed. This technique, combining the strengths of well known standard fabrication techniques with the ease of self-folding, could have many applications, such as 3D sensing, Micro-Opto-Electro-Mechanical Systems (MOEMS), or 3D memory.

Furthermore, we have shown that the use of corner lithography leads to retraction in all three dimensions (Fig 9). For the purpose of self-folding, only the features at the bottom of the molds were used, the others being etched away in Fig 4(j). Other features might be of interest for different purposes. For example, unique 3D membranes or channels could be obtained. Several applications have already been developed using corner lithography, such as the wafer scale fabrication of nano-apertures [46, 47], photonic crystals [44] or micro-cages in which the culture of bovine cells has been demonstrated [45].

Conclusions

Starting from a simple micrometer-sized mask, accurate stop-programmable hinges for complex elastocapillary folding were micromachined in three dimensions using corner lithography. In order to limit the stress in the hinges while folding, it was necessary to start with round molds. Corner lithography can be performed only if the combined thicknesses of the two first deposited layers is greater than the radius of curvature of the mold. When this design criterion is respected, material can be accurately etched starting from any concave corner, independently of their spatial orientation.

The definition of the silicon molds at the start of the process determines both the locking angle and the accuracy of the stop-programmable hinges. Selective KOH etching on (110) wafers yields well defined sharp corners that, in turn, can be used to micro-machine smart hinges that stop folding at 70.6(01)°. Micrometer sized three dimensional tetrahedral structures were successfully self-folded using capillary forces, thanks to these hinges.

We demonstrated the feasibility of 90° stop-programmable hinges. Such complex hinges can be fabricated by making initial molds with dry etching at the cost of a poorer accuracy 89 (4)° compared to wet etching. Extra care must be taken when using dry etching to avoid any undesirable sharp corners, and a long over-etching during corner lithography must be performed to remove unwanted material. Moreover, small irregularities in the molds will be magnified by the process and will cause defects in the final shape of the flaps.

Stop-programmable hinges extend the possibilities for implementing the elasto-capillary folding of microstructures. Using a simple filling procedure, millimeter-long silicon-based structures can be accurately popped out of the plane. We believe that the accuracy and versatility of the technique will find widespread application in 3D sensing, MOEMS, or 3D electronics, for instance.

Acknowledgments

The authors would like to thank R. G. P. Sanders for his valuable help with the folding experiments, K. Ma for his precious help with the cleanroom work, and M. J. de Boer for his advice on dry etching. This paper would have never been possible without J. W. van Honschoten, who inspired this project.

Author Contributions

Conceived and designed the experiments: AL EB NT LA. Performed the experiments: AL EB. Analyzed the data: AL EB NT LA. Wrote the paper: AL EB NT LA.

References

1. Leong TG, Zarafshar AM, Gracias DH (2010) Three-dimensional fabrication at small size scales. Small 6: 792–806. doi: 10.1002/smll.200901704 PMID: 20349446
2. Madou MJ (1997) Fundamentals of Microfabrication. CRC Press, New York.
3. Shin C (2014) State-of-the-art silicon device miniaturization technology and its challenges. IEICE Electronics Express 11.
4. Sugioka K, Xu J, Wu D, Hanada Y, Wang Z, et al. (2014) Femtosecond laser 3d micromachining: a powerful tool for the fabrication of microfluidic, optofluidic, and electrofluidic devices based on glass. Lab Chip 14: 3447–3458. doi: 10.1039/C4LC00548A PMID: 25012238
5. Gattass RR, Mazur E (2008) Femtosecond laser micromachining in transparent materials. Nature photonics 2: 219–225. doi: 10.1038/nphoton.2008.47
6. Whitesides GM, Grzybowski B (2002) Self-assembly at all scales. Science 295: 2418–2421. doi: 10.1126/science.1070821 PMID: 11923529
7. Ariga K, Hill JP, Lee MV, Vinu A, Charvet R, et al. (2008) Challenges and breakthroughs in recent research on self-assembly. Science and Technology of Advanced Materials 9: 014109. doi: 10.1088/1468-6996/9/1/014109
8. Mastrangeli M, Abbasi S, Varel C, van Hoof C, Celis JP, et al. (2009) Self-assembly from milli- to nanoscales: methods and applications. Journal of Micromechanics and Microengineering 19: 1–37. doi: 10.1088/0960-1317/19/8/083001
9. Brittain ST, Schneller OJA, Wu H, Whitesides S, Whitesides GM (2001) Microorigami: Fabrication of small, three-dimensional, metallic structures. The Journal of Physical Chemistry B 105: 347–350. doi: 10.1021/jp002556e
10. Kaajakari V, Lal A (2003) Thermokinetic actuation for batch assembly of microscale hinged structures. Microelectromechanical Systems, Journal of 12: 425–432. doi: 10.1109/JMEMS.2003.811747
11. Lu YW, Kim CJ (2006) Microhand for biological applications. Applied Physics Letters 89: 164101. doi: 10.1063/1.2362602
12. Guan J, He H, Hansford DJ, Lee LJ (2005) Self-folding of three-dimensional hydrogel microstructures. The Journal of Physical Chemistry B 109: 23134–23137. doi: 10.1021/jp054341g PMID: 16375273
13. Kim SJ, Kim HI, Park SJ, Kim IY, Lee SH, et al. (2005) Behavior in electric fields of smart hydrogels with potential application as bio-inspired actuators. Smart Materials and Structures 14: 511. doi: 10.1088/0964-1726/14/4/008
14. Luo J, Huang R, He J, Fu Y, Flewitt A, et al. (2006) Modelling and fabrication of low operation temperature microcages with a polymer/metal/dlc trilayer structure. Sensors and Actuators A: Physical 132: 346–353. doi: 10.1016/j.sna.2006.03.004
15. Stoychev G, Puretskiy N, Ionov L (2011) Self-folding all-polymer thermoresponsive microcapsules. Soft Matter 7: 3277–3279. doi: 10.1039/c1sm05109a
16. Ionov L (2011) Soft microorigami: self-folding polymer films. Soft Matter 7: 6786–6791. doi: 10.1039/c1sm05476g

17. Liu Y, Boyles JK, Genzer J, Dickey MD (2012) Self-folding of polymer sheets using local light absorption. Soft Matter 8: 1764–1769. doi: 10.1039/C1SM06564E
18. Arora WJ, Nichol AJ, Smith HI, Barbastathis G (2006) Membrane folding to achieve three-dimensional nanostructures: Nanopatterned silicon nitride folded with stressed chromium hinges. Applied Physics Letters 88: 1–3. doi: 10.1063/1.2168516
19. Schmidt OG, Eberl K (2001) Nanotechnology: Thin solid films roll up into nanotubes. Nature 410: 168–168. doi: 10.1038/35065525 PMID: 11242068
20. Chua C, Fork D, Van Schuylenbergh K, Lu JP (2003) Out-of-plane high-q inductors on low-resistance silicon. Microelectromechanical Systems, Journal of 12: 989–995. doi: 10.1109/JMEMS.2003.820274
21. Leong TG, Benson BR, Call EK, Gracias DH (2008) Thin film stress driven self-folding of microstructured containers. Small 4: 1605–1609. doi: 10.1002/smll.200800280 PMID: 18702125
22. Cho JH, James T, Gracias DH (2010) Curving nanostructures using extrinsic stress. Advanced Materials 22: 2320–2324. doi: 10.1002/adma.200904410 PMID: 20376856
23. Judy J, Muller R (1997) Magnetically actuated, addressable microstructures. Microelectromechanical Systems, Journal of 6: 249–256. doi: 10.1109/84.623114
24. Boncheva M, Andreev SA, Mahadevan L, Winkleman A, Reichman DR, et al. (2005) Magnetic self-assembly of three-dimensional surfaces from planar sheets. Proceedings of the National Academy of Sciences 102: 3924–3929. doi: 10.1073/pnas.0500807102
25. Iwase E, Shimoyama I (2006) A design method for out-of-plane structures by multi-step magnetic self-assembly. Sensors and Actuators A: Physical 127: 310–315. doi: 10.1016/j.sna.2006.01.025
26. Nichol AJ, Arora WJ, Barbastathis G (2006) Thin membrane self-alignment using nanomagnets for three-dimensional nanomanufacturing. Journal of Vacuum Science & Technology B 24: 3128–3132. doi: 10.1116/1.2375084
27. Gagler R, Bugacov A, Koel BE, Will PM (2008) Voxels: volume-enclosing microstructures. Journal of Micromechanics and Microengineering 18: 055025. doi: 10.1088/0960-1317/18/5/055025
28. Syms R, Yeatman E (1993) Self-assembly of three-dimensional microstructures using rotation by surface tension forces. Electronics Letters 29: 662–664. doi: 10.1049/el:19930444
29. Syms R (2000) Self-assembled 3-D silicon microscanners with self-assembled electrostatic drives. Photonics Technology Letters, IEEE 12: 1519–1521. doi: 10.1109/68.887729
30. Leong TG, Lester PA, Koh TL, Call EK, Gracias DH (2007) Surface tension-driven self-folding polyhedra. Langmuir 23: 8747–8751. doi: 10.1021/la700913m PMID: 17608507
31. Filipiak DJ, Azam A, Leong TG, Gracias DH (2009) Hierarchical self-assembly of complex polyhedral microcontainers. Journal of Micromechanics and Microengineering 19: 075012. doi: 10.1088/0960-1317/19/7/075012
32. Cho JH, Gracias DH (2009) Self-Assembly of lithographically patterned nanoparticles. Nano Letters 9: 4049–4052. doi: 10.1021/nl9022176 PMID: 19681638
33. Randall CL, Gultepe E, Gracias DH (2011) Self-folding devices and materials for biomedical applications. Trends in Biotechnology 30: 138–146. doi: 10.1016/j.tibtech.2011.06.013 PMID: 21764161
34. Shenoy VB, Gracias DH (2012) Self-folding thin-film materials: From nanopolyhedra to graphene origami. MRS Bulletin 37: 847–854. doi: 10.1557/mrs.2012.184
35. Ionov L (2013) Bioinspired microorigami by self-folding polymer films. Macromolecular Chemistry and Physics 214: 1178–1183. doi: 10.1002/macp.201200246
36. Py C, Reverdy P, Doppler L, Bico J, Roman B, et al. (2007) Capillary origami: Spontaneous wrapping of a droplet with an elastic sheet. Physics Review Letters 98: 156103. doi: 10.1103/PhysRevLett.98.156103
37. Py C, Reverdy P, Doppler L, Bico J, Roman B, et al. (2009) Capillarity induced folding of elastic sheets. The European Physical Journal—Special Topics 166: 67–71. doi: 10.1140/epjst/e2009-00880-4
38. Roman B, Bico J (2010) Elasto-capillarity: deforming an elastic structure with a liquid droplet. Journal of Physics: Condensed Matter 22: 493101. PMID: 21406780
39. van Honschoten JW, Berenschot JW Ondarçuhu T, Sanders RGP, Sundaram J, et al. (2010) Elastocapillary fabrication of three-dimensional microstructures. Applied Physics Letters 97: 0141031–0141033. doi: 10.1063/1.3462302
40. Legrain A, Janson TG, Berenschot JW, Abelmann L, Tas NR (2014) Controllable elastocapillary folding of three-dimensional micro-objects by through-wafer filling. Journal of Applied Physics 115: 214905. doi: 10.1063/1.4878460
41. Syms R, Yeatman EM, Bright VM, Whitesides GM (2003) Surface tension-powered self-assembly of microstructures—the state-of-the-art. Microelectromechanical Systems, Journal of 12: 387–417. doi: 10.1109/JMEMS.2003.811724

42. Sarajlic E, Berenschot JW, Krijnen GJM, Elwenspoek MC (2005) Fabrication of 3D nanowire frames by conventional micromachining technology. In: 13th Int. Conf. on Solid-State Sensors, Actuators and Microsystems, Digest of Technical Papers (TRANSDUCERS '05). Seoul, South Korea, volume 1, pp. 27–30.

43. Berenschot E, Tas NR, Jansen HV, Elwenspoek M (2008) 3D-nanomachining using corner lithography. In: 3rd IEEE Int. Conf. on Nano/Micro Engineered and Molecular Systems (NEMS 2008). Sanya, pp. 729–732.

44. Yu X, Zhang H, Oliverio JK, Braun PV (2009) Template-assisted three-dimensional nanolithography via geometrically irreversible processing. Nano Letters 9: 4424–4427. doi: 10.1021/nl9027236 PMID: 19921779

45. Berenschot EJW, Burouni N, Schurink B, van Honschoten JW, Sanders RGP, et al. (2012) 3D nanofabrication of fluidic components by corner lithography. Small 8: 3823–3831. doi: 10.1002/smll.201290137 PMID: 22907803

46. Burouni N, Berenschot E, Elwenspoek M, Sarajlic E, Leussink P, et al. (2013) Wafer-scale fabrication of nanoapertures using corner lithography. Nanotechnology 24: 285303. doi: 10.1088/0957-4484/24/28/285303 PMID: 23792365

47. Berenschot EJW, Jansen HV, Tas NR (2013) Fabrication of 3D fractal structures using nanoscale anisotropic etching of single crystalline silicon. Journal of Micromechanics and Microengineering 23: 055024. doi: 10.1088/0960-1317/23/5/055024

48. Sinclair G, Kondo M (1984) On the stress concentration at sharp re-entrant corners in plates. International Journal of Mechanical Sciences 26: 477–487. doi: 10.1016/0020-7403(84)90002-X

49. Pilkey W, Pilkey D (2008) Peterson's Stress Concentration Factors. Wiley. URL http://books.google.nl/books?id=JUAdYkKh0V8C.

50. Gardeniers JGE, Tilmans HAC, Visser CCG (1996) LPCVD silicon-rich silicon nitride films for applications in micromechanics, studied with statistical experimental design. J Vac Sci Technol, A 14: 2879–2892. doi: 10.1116/1.580239

51. Kim G, Kovalgin A, Holleman J, Brugger J (2002) Replication molds having nanometer-scale shape control fabricated by means of oxidation and etching. Journal of Nanoscience and Nanotechnology 2: 55–9. doi: 10.1166/jnn.2002.073 PMID: 12908321

52. Shankoff T, Sheng T, Haszko S, Marcus R, Smith T (1980) Bird's beak configuration and elimination of gate oxide thinning produced during selective oxidation. Journal of the Electrochemical Society 127: 216–222. doi: 10.1149/1.2129621

53. Landau LD, Kosevich AM, Lifshitz EM (1986) Theory of Elasticity. Butterworth-Heinemann, 196 pp.

54. Jansen HV, De Boer MJ, Unnikrishnan S, Louwerse MC, Elwenspoek MC (2009) Black silicon method X: a review on high speed and selective plasma etching of silicon with profile control: an in-depth comparison between Bosch and cryostat DRIE processes as a roadmap to next generation equipment. Journal of Micromechanics and Microengineering 19: 033001. doi: 10.1088/0960-1317/19/3/033001

55. Tas N, Sonnenberg T, Jansen H, Legtenberg R, Elwenspoek M (1996) Stiction in surface micromachining. J Micromech Microeng 6: 385–397. doi: 10.1088/0960-1317/6/4/005